Glass formation and characterization in the $3Al_2O_3 \cdot 2SiO_2$-$LaPO_4$ system

Shuling Guo-Malloy[a], Paul F. McMillan[b] and William T. Petuskey[a, c,*]

[a] Science and Engineering of Materials, Arizona State University, Tempe, Arizona 85287-1704, USA

[b] Department of Chemistry, University College London, 20 Gordon Street, London WC1H 0AJ, UK

[c] School of Molecular Sciences, Arizona State University, Tempe, Arizona 85287-1604, USA

* Corresponding Author: wpetuskey@asu.edu

Abstract

Rare earth oxide-aluminate-phosphate-silicate (REAPS) glasses are useful precursors for ceramic matrix composites (CMCs) with important thermal and mechanical properties. It is important to determine the glass structure, relaxation and crystallization properties for designing and controlling CMC formation. Transparent $3Al_2O_3 \cdot 2SiO_2$-$LaPO_4$ glasses containing 25-80 mol% mullite ($3Al_2O_3 \cdot 2SiO_2$) component were prepared by quenching from high temperature melts using a containerless technique. Glass transformation and crystallization behavior were examined by differential scanning calorimetry and X-ray diffraction. The glass transition onset increased from 845 to 906°C with mullite content. The temperature interval between T_g and crystallization was maximized at 200°C for 50 mol% mullite glass. Below 40 mol% mullite, successive appearance of $LaPO_4$ (monazite) and mullite gave rise to two crystallization peaks, while at higher mullite content, only one combined exotherm was observed. A glass structure model constructed from ^{27}Al, ^{31}P and ^{29}Si magic angle spinning (MAS) NMR and Raman spectroscopy results indicated that Si^{4+} and P^{5+} remained tetrahedrally bonded while Al^{3+} ions were predominantly in four-fold coordination with some five-coordinated sites. The presence of La_2O_3 component resulted in an increased proportion of AlO_4 tetrahedra. The PO_4 polymerization state varied from Q^3 to Q^2 with increasing $LaPO_4$ content. The SiO_4, AlO_4, and PO_4 units form a continuous network with PO_4 tetrahedra attached to aluminosilicate framework through two or three P-O-Al linkages. SiO_4 tetrahedra crosslink with AlO_4 tetrahedra to form $Q^4(4Al)$ and $Q^4(3Al)$ units. The glass structure model helps explain the crystallization sequence as a function of mullite content and the formation of different CMC textures.

1. Introduction

Lanthanum phosphate monazite ($LaPO_4$) has received attention for applications in high temperature structural ceramics because of its ability to facilitate debonding between the matrix and reinforcements as required for fracture damage tolerance in ceramic-matrix-composites (CMCs) [1-3]. Many oxide/oxide composites intended for high temperature structural materials are fabricated from fibers and matrices based on mullite ($3Al_2O_3{\cdot}2SiO_2$ ideal composition) due to the favorable high temperature properties of this ceramic phase [4]. Glass-ceramics based on mullite along with apatite ($Ca_5(PO_4)_3(OH,F)$) or fluorite (CaF_2) are important for biomedical implant technology [5, 6]. Building on the proven high temperature stability and compatibility of La-monazite with crystalline mullite [1, 7], the low fracture strength at the interface between the two phases [8] is a highly attractive property appropriate for blunting crack propagation in oxide/oxide composite materials. We are now investigating the ability of $3Al_2O_3{\cdot}2SiO_2$-$LaPO_4$ glasses to be developed as fully dense precursors for fabricating ceramic-matrix-composites (CMCs) based within the rare earth oxide-aluminate-phosphate-silicate (REAPS) systems to provide functional micro- to nanoscale structures *via* controlled nucleation and growth processing [9]. Implementing this requires an understanding of the glass formation and atomic level structures in relation to their relaxation and crystallization properties in order to design, and properties precursors leading to, composites with the desired micro- to nanoscale textures.

In the system examined here, three network-forming oxides, SiO_2, Al_2O_3, and P_2O_5, were combined together along with a network-modifying component, La_2O_3, in various ratios along the compositional join between mullite ($3Al_2O_3{\cdot}2SiO_2$) and monazite ($LaPO_4$). The structural roles of Al_2O_3, SiO_2, and P_2O_5 components in alkali-alkaline earth-alumina-silica glasses have been investigated extensively using vibrational and ^{27}Al, ^{31}P and ^{29}Si MAS NMR spectroscopy

[10-15]. Varying the P_2O_5 content in Na- or K- silicate glasses results in formation of ortho- (PO_4^{3-}), pyro- ($P_2O_7^{4-}$), and metaphosphate ($[PO_3^-]_n$) chain units [10]. At high P_2O_5 concentrations, the SiO_2 component is either incorporated into sodium phosphate glass as chain terminating species ($-OSiO_3^{3-}$), or else it contributes to the appearance of a crystalline SiP_2O_7 phase containing octahedrally-bonded SiO_6 [10]. Substitution of Al_2O_3 for P_2O_5 suppresses formation of the SiP_2O_7 phase, and a tetrahedrally-coordinated SiO_2-rich glassy component separates out from the phosphate and aluminophosphate networks [11]. At high SiO_2 concentrations and with $Al_2O_3 >> P_2O_5$ content, the phosphate component resides mainly within an $AlPO_4$-type environment outside the aluminosilicate framework [14, 16, 17].

In the present study, transparent $3Al_2O_3 \cdot 2SiO_2$-$LaPO_4$ glasses containing 25-100 mol% mullite component were readily prepared by rapid (10^3-10^4 $^oC/s$) quenching from the high temperature liquids using a containerless technique [18-20]. The glass structures were investigated using ^{27}Al, ^{29}Si and ^{31}P magic angle spinning nuclear magnetic resonance (MAS NMR) and Raman spectroscopy, and their relaxation and crystallization properties were established by differential scanning calorimetry (DSC) and powder X-ray diffraction (XRD). Structural models established from the spectroscopic results allowed an understanding of the arrangement and linkages between cations and their coordination states in REAPS glasses that were used to rationalize the crystallization behavior and glass properties.

2. Experimental

Reagent grade mullite (60 mol% Al_2O_3, Alfa Aesar) and $LaPO_4$ (Alfa Aesar) were ground and mixed in an agate mortar. After sintering and re-grinding, the mixture was packed into a rod-forming mold, isostatically cold pressed at 4,500 psi, and sintered at 1200°C overnight. By

melting the tip of the sintered rod in a xenon-arc image furnace (NEC SC-30XS), liquid droplets fell through a platinum grid, forming smaller droplets, which were then rapidly quenched in water. The quench rate was estimated to be between 10^3-10^4 °C/sec. The procedure has been described in detail previously[18-20].

Glass compositions were determined by wavelength-dispersive electron probe microanalysis (JEOL JXA-8600) at 20 keV with beam current 10 nA using a ~1 μm diameter electron beam (Table 1). Crystalline apatite, corundum, olivine, and $LaAlO_3$ were used as standards. Measurements were obtained on glass spheroids for each composition at several points across the diameter of the polished and carbon-coated surface. The density was measured by He displacement pycnometry (Micromeretics AccuPyc 1330) calibrated using Si and Bi standards. Powder X-ray diffraction patterns were obtained using a Siemens D5000 diffractometer (40 kV, 30 mA) using Cu K_α radiation. DSC experiments were carried out with 60-65 mg glass powder (< 50 μm mesh) placed in an Al_2O_3 pan using a Netzsch STA 449 C "Jupiter" thermal analyzer. Continuous scans of the baseline, standard, and sample were performed at 20°C/min to 1400 °C in flowing N_2 (50 mL/min).

^{31}P MAS NMR spectra were collected using a 4 mm Jakobsen MAS probe in a Varian Innova 400 spectrometer operating at 79.5 MHz. Spectra were obtained on samples spinning at 12 kHz in a Si_3N_4 rotor, with a 3.0 μs π/2 pulse and 60 s recycle delay. Chemical shifts were referenced to 1 M aqueous H_3PO_4. ^{29}Si MAS NMR spectra were obtained at a Larmor frequency of 162.0 MHz, using 7.0 or 7.5 kHz spinning rate, a 3.0 μs π/2 pulse, and a 5.0 s recycle delay. The Si_3N_4 rotor (δ= -48.5 ppm relative to TMS) was used to calibrate ^{29}Si peak positions. ^{27}Al MAS NMR spectra were collected at 104.2 MHz using a 12 kHz spinning rate in a Si_3N_4 rotor, a 1.2 μs π/2 pulse, and a 1 s recycle delay, and referenced to 1 M aqueous $AlCl_3$. Raman spectra

were obtained using a Jobin Yvon Triax 550 spectrometer with LN2 cooled CCD detection coupled to an Olympus BH-2 microscope fitted with a Mitutoyo long working distance 50x objective and excited by 514.5 nm Ar^+ laser radiation.

3. Results

3.1. Glass Formation, Composition and Density

We typically observed some loss of the volatile P_2O_5 component from the high temperature liquids prior to quenching so that the analyzed glass compositions deviated slightly from the starting glass mixtures along the $LaPO_4$-mullite join [21] (Table 1). Vaporization losses of P_2O_5 component were generally <15% of the total amount present in the initial mixture. This contrasts with quenched Al_2O_3-$AlPO_4$ glasses prepared previously that exhibited 35-45 mol% P_2O_5 losses [21]. However, the Al/Si ratio remained constant at 3:1 throughout the series. For simplicity we retain the use of the starting compositions to describe and designate the samples obtained in the study.

For samples containing between 25-80 mol% mullite ($3Al_2O_3 \cdot 2SiO_2$) component, crystal-free glass beads formed readily by quenching from the melts using the containerless technique described above. The powder X-ray diffraction patterns of these samples exhibited only the broad diffraction features characteristic of amorphous materials (Fig 1). For compositions containing <25 mol% mullite significant crystallization occurred during the quench and the patterns were dominated by sharp diffraction peaks identified as $LaPO_4$ monazite. At high (>80%) mullite content, crystallization occurred in most of our synthesis attempts resulting in a mixture of monazite + mullite or pure mullite phases. However, in some experiments, we also obtained spheres of completely glassy material at the pure mullite ($3Al_2O_3 \cdot 2SiO_2$) composition

(Fig. 1). In previous studies of glass formation along the Al_2O_3-SiO_2 join, hammer- or roller-quenching techniques with quench rates of up to 10^4-10^6 $^oC/s$ were used to obtain high alumina glasses[22-25].***

The glass densities are lower than those of the corresponding crystalline mixtures, and they decrease with increasing mullite content showing an upward trend in density as the mullite content is reduced below 50% (Table 1, Fig. 2). The largest separation between the glass density and that of the arithmetic mean of the crystalline monazite + mullite phases occurs at the 50% mullite composition. The density of pure mullite glass (2.824 g/cm^3) obtained in our study is close to that measured for sample prepared from coal ash (2.81 g/cm^3 : **[26]**), that is ~13% lower than crystalline $3Al_2O_3 \cdot 2SiO_2$ (Fig. 2).

3.2. Differential scanning calorimetry (DSC): glass transitions and crystallization exotherms

DSC traces of $3Al_2O_3 \cdot 2SiO_2$-$LaPO_4$ glasses heated at 20°C/min exhibited a small initial endothermic rise that we associate with the onset of T_g within the range 840 to 910°C followed by either one or two sharp exotherms depending on the sample composition (Fig. 3). The T_g onset value increases linearly from 845 to 906°C with mullite content between 25-80 mol% (Fig. 4). No obvious endotherm was apparent for pure mullite glass although a slight change in background slope occurred near 930°C, close to the T_g value determined by [26] (920^{o}C) (Fig 3). We note the unusual shape of the endothermic signal for glasses with 50-60% mullite that appear to show a plateau between the T_g onset and the exothermic crystallization event. We present a possible model to explain this behavior below.

A single crystallization exotherm was observed for glasses with >35 mol % mullite, whereas two exotherms appeared for compositions with 20-35 mol% $3Al_2O_3 \cdot 2SiO_2$ content. The

crystallization behavior observed for the glassy samples by powder X-ray diffraction also adopts two different patterns, depending on the composition range. For compositions with <35 mol% mullite, the two exothermic events are accompanied by crystallization of $LaPO_4$ (T_{x1} = 903-959°C) and mullite (T_{x2} = 987-998°C), respectively (Table 1). We have summarized the results in Fig. 4, differentiating between "concurrent" *vs* "separate" crystallization of the mullite and monazite components based on the DSC exotherms. Below 35 mol% mullite, the monazite crystallization temperature (T_{x1}) decreases rapidly with increasing $LaPO_4$ concentration, whereas crystallization of the mullite component occurs at approximately the same temperature as for pure $Al_6Si_2O_{13}$ glass (992˚C) (Fig. 4). In the "concurrent" regime the peak crystallization temperature reaches a maximum of 1064°C at 50 mol % mullite. As the mullite content continues to increase, T_x decreases to 1015°C for 80 mol% mullite glass, and smoothly extrapolates to 992°C for the pure aluminosilicate glass. No crystal-free glasses could be obtained for $LaPO_4$-$3Al_2O_3 \cdot 2SiO_2$ compositions below 25 mol% mullite. However, extrapolating from our data allows us to estimate that convergence between T_g and T_{x1} (T_x) should occur between 820-830^{o}C for very high monazite-containing glasses, if these could be prepared. Understanding the crossover between “separate” *vs* “concurrent” crystallization regimes is important for developing the CMC textures consisting of interlocking mullite and La-monazite phases from within the REAPS glass matrix. The local structural units present within the glass are likely to play a key role in determining this behavior.

3.3. MAS NMR and Raman spectroscopic studies of $3Al_2O_3 \cdot 2SiO_2$-$LaPO_4$ glasses

The ^{27}Al spectrum of high alumina glasses including the mullite composition typically show three resonances near +60, +30 and 0 ppm that are assigned to 4-, 5- and 6-coordinated

AlO_n species, respectively[17, 24, 25, 27, 28]. The mullite glass prepared in this study showed all three of these peaks. The AlO_6 contribution diminished rapidly as the $LaPO_4$ content was increased, and between 25-60% mullite the glass structures appear to be dominated by AlO_4 units (Fig. 5a). We could report ^{27}Al, as well as, ^{29}Si MAS NMR spectra for the remaining glassy component within the partly crystalline 20% mullite sample, as the crystalline phase produced was pure $LaPO_4$ monazite. This glass shows a more prominent AlO_5 signal and a contribution from AlO_6 units can also be detected once more. This result is consistent with the removal of $LaPO_4$ component from the glassy matrix.

The ^{29}Si MAS NMR spectra of $3Al_2O_3{\cdot}2SiO_2$-$LaPO_4$ glasses exhibit a main peak that shifts its maximum slightly from –84 to –90 ppm with increasing mullite content (Fig. 5b). The strong peak at –48.5 ppm is due to the Si_3N_4 rotor that also provides the spinning side bands (spinning speeds 7.5 or 7.0 kHz) observed at –140 to -130 ppm. In aluminosilicate glasses, ^{29}Si chemical shifts between -83 and -85 ppm are typically assigned to fully polymerized SiO_4 units with their bridging oxygens linked to four Al^{3+} cations (i.e., $Q^4(4Al)$ units), and those between -88 to -94 ppm to $Q^4(3Al)$ species [29]. Our analysis suggests that in these REAPS glasses the SiO_4 tetrahedra crosslink with four Al as next nearest neighbors at low mullite contents, and with 3 Al + 1 Si as next nearest neighbors for high mullite compositions. For many of the glasses, a second small peak appears near -110 ppm, that usually indicates the presence of nearly pure SiO_2 domains within the glassy matrix. That observation is discussed below along with interpretation of the DSC results. We found no evidence for Si–O–P linkage formation that would have resulted in significantly more negative chemical shift values in the ^{29}Si MAS NMR spectra [10, 30, 31].

The ^{31}P MAS NMR spectrum of the partly recrystallized 20 mol% mullite sample shows only a single sharp resonance at -2 ppm due to crystalline $LaPO_4$. That indicates that most of the phosphate component has been removed from the glassy matrix *via* La-monazite crystallization (Fig. 5c). The 25 mol% glass also shows a weak shoulder near this position superimposed on the glassy resonance centered at -10 ppm, indicating that a small quantity of crystals is present in this sample also. For 50-80% mullite samples the ^{31}P chemical shift changes between -23 to -17 ppm. Extrapolating the linear trend toward even lower $LaPO_4$ contents indicates a limiting chemical shift near values for crystalline $AlPO_4$ (-27 ppm) [32] or amorphous $63Al_2O_3 \cdot 37AlPO_4$ (-24 ppm) [21] (Fig. 6). This observation indicates that tetrahedrally bonded PO_4 units in the glass are mainly surrounded by Al^{3+} cations at high mullite concentrations. No chemical shifts occur with more negative values (e.g., < -32 ppm) are observed confirming the absence of P-O-Si linkages as also indicated by the ^{29}Si MAS NMR data [10, 15]. A break in slope of the ^{31}P chemical shift *vs* phosphate content occurs between 50-75 mol% $LaPO_4$ (25-50% mullite) compositions (Fig. 6). The chemical shifts increase rapidly from -15 to -7 ppm for the highest phosphate content glass, only slightly lower than that for crystalline $LaPO_4$ monazite (-4 ppm) [33]. That observation indicates a rapid change in the local glass structure occurs at around the 50 mol% mullite composition, as the PO_4 units become increasingly surrounded by La^{3+} cations replacing Al^{3+} in the next-nearest neighbor environments surrounding the phosphate groups. Interesting, the ^{31}P chemical shift (-2 ppm) recorded for the crystalline $LaPO_4$ material within the partially recrystallized 20% mullite glass occurs at a less negative value than that for bulk La-monazite crystal (Fig. 7).

The Raman spectrum of the partially recrystallized 20% mullite sample is dominated by sharp peaks arising from crystalline $LaPO_4$ monazite (Fig. 8). As the mullite content increases,

the strong tetrahedral P-O stretching bands near 1000 cm^{-1} broaden and merge into a single main feature that shifts to higher wavenumber as the $LaPO_4$ content decreases and network-forming P-O-Al linkages replace the more ionic interactions between PO_4^{3-} units and La^{3+} cations. At the same time, (Al,Si)-O stretching bands appear in the 900-1200 cm^{-1} region of the spectrum [22-24]. The PO_4 bending vibrations observed near 400 cm^{-1} for crystalline $LaPO_4$ remain visible as a distinct, but broadened band in the glass spectra until approximately 40% mullite concentration. A further broad feature in the 550-750 cm^{-1} region accounts for contributions from vibrations of the network cations Si^{4+}, Al^{3+} and P^{5+} relative to their mainly tetrahedral sites defined by the O^{2-} glassy matrix sublattice.

4. Discussion

We combined the results of our spectroscopic and DSC investigations to propose a structural model for the REAPS glasses that can aid in understanding and controlling the glass relaxation and recrystallization behavior. Our model is based on mainly tetrahedral SiO_4, AlO_4, and PO_4 units that are linked *via* bridging oxygens (BO) to form a continuous glass network. The REAPS glasses do not provide a completely random arrangement of these three species. The PO_4 units are attached *via* 2-3 BO to mainly AlO_4 tetrahedra with some contribution from AlO_5 groups, whereas Q^4(4Al) and Q^4(3Al) units occur within the aluminosilicate network, as expected thermodynamically[34-37]. Al-O-P and Al-O-Si linkages are thus favored over P-O-P, P-O-Si, and possibly even Si-O-Si linkages, although that point is discussed in more detail below. Linking together the AlO_4 and PO_4 units tends to stabilize the aluminate and phosphate tetrahedra within the glass network as the 5+ and 3+ valencies of P and Al provide appropriate local charge compensation at the bridging oxygen (BO) sites [38]. Formation of P-O-Si bonds is

not favored due to the potential overbonding at BOs, but a reduction of local electrostatic repulsion occurs by inserting AlO_4 tetrahedra between PO_4 and SiO_4 tetrahedra in the glass network. The absence of ^{31}P NMR resonances at ~27 ppm indicates that no tetrahedrally coordinated $Q^4(4Al)$ PO_4^{3-} groups such as might be found in $AlPO_4$ units are present in the REAPS glasses. Adding La_2O_3 component to the glass matrix preferentially depolymerizes phosphate tetrahedra from Q^3 (three BO) to Q^2 (two BO) species by increasing the number of non-bridging oxygens (NBO) present. We thus infer that the phosphate tetrahedra lie at the edges of domains within the tetrahedral aluminosilicate framework, and are attached to that matrix *via* 2-3 BO linked with AlO_4 tetrahedra (Fig. 9). The stabilization of AlO_4 tetrahedra by the addition of La_2O_3 component has also been suggested to occur in La-aluminosilicate glasses [39] and Al_2O_3-$LaPO_4$ liquids [18].

The high T_g values for $3Al_2O_3{\cdot}2SiO_2$-$LaPO_4$ glasses (835-905˚C) are typical of oxide systems. They decrease as a function of $LaPO_4$ content as the addition of the network modifier decreases the average polymerization, and increase with mullite content containing the network forming species Al_2O_3 and SiO_2 [39]. The crystallization behavior of $3Al_2O_3{\cdot}2SiO_2$-$LaPO_4$ glasses is affected by the addition of $LaPO_4$ component in two ways. The formation of Al-O-P linkages results in increased network polymerization, whereas added La_2O_3 component increases the NBO content of the phosphate tetrahedra as discussed above.

We suggest that formation of Al-O-P bonds results in the increased crystallization temperature (T_x) observed with increasing $LaPO_4$ content as the composition is changed between 100-50% mullite (Fig. 4). At this composition the number of Al–O–P bonds is maximized, which subsequently decreases at even higher $LaPO_4$ contents. At the highest point, the crystallization temperature reaches 1064^{o}C. Here, the glass structure exhibits a maximum degree

of network polymerization, resulting in a lowered viscosity and kinetically hindering any intrinsic thermodynamic driving force to segregate into $LaPO_4$ and aluminosilicate-rich phases. The wide T_x-T_g temperature interval achieved at this point is critical for sintering of glasses to eliminate free surfaces by viscous flow and allowing separate control of crystal nucleation and growth rates. As the $LaPO_4$ content exceeds 50 mol%, the strengthening effects of Al-O-P bond formation are counteracted by network depolymerization and increased formation of PO_4 tetrahedra surrounded by La^{3+} ions. These imply an enhanced tendency to crystallize the thermodynamically stable La-monazite phase coupled with segregation of the supercooled liquid above T_g into an aluminosilicate-rich component that yields crystalline mullite (Fig. 4).

In our presentation of the DSC results above, we noted that immediately following the onset of the glass transformation range at T_g, an unexpected plateau was observed in the endothermic signal for 50-60% mullite glasses before the crystallization exotherm (Fig. 3). Following analysis of the glass formation and crystallization behavior of a wide range of compositions within the La_2O_3-Al_2O_3-P_2O_5-SiO_2 REAPS system and detailed nanoscale analysis of the products formed, we can now suggest that this unusual thermal signature could be related to incipient chemical unmixing and segregation of components within the supercooled liquid phase. That possibility leads to an even wider range of controllable nano- to microscale structures that could be developed within the resulting CMCs. Those concepts will be discussed in a following communication.

5. Conclusions

A series of transparent $3Al_2O_3 \cdot 2SiO_2$-$LaPO_4$ glasses with 20-75 mol% initial mullite concentration were prepared from melts quenched from the corresponding liquids using a

containerless technique. Overall, our study has established the basis for glass formation within the La_2O_3-Al_2O_3-P_2O_5-SiO_2 (REAPS) system leading to CMCs with potentially important properties. Based on spectroscopic and DSC measurements, the following conclusions have been made concerning the nature of the glass matrix structure that we envisage will provide a fully dense precursor for CMC production following thermal processing:

(1) The glass matrix is based on interconnected SiO_4, PO_4 and mainly AlO_4 units linked *via* SiOSi, AlOSi, and AlOP linkages. Some AlOAl linkages may be present, but SiOP linkages are absent. PO_4 tetrahedra attach to the aluminosilicate framework through two or three P-O-Al linkages.

(2) SiO_4 tetrahedra crosslink with 3 or 4 AlO_4 tetrahedra producing Q^4 (4Al) and Q^4 (3Al) species. The polymerization of PO_4 tetrahedra varies from Q^3 to Q^1 with increasing $LaPO_4$ content. La_2O_3 preferentially depolymerizes PO_4 tetrahedra and stabilizes AlO_4 tetrahedra.

(4) The glass transition temperature increases systematically from 845 to approximately 903°C as the starting mullite concentration changes from 25-100 mol%. Crystallization of $LaPO_4$ and mullite occurs as two separate events (T_{x1}, T_{x2}, respectively) for samples between 25-35% mullite, followed by a concurrent crystallization regime (T_x) for glasses with higher mullite concentration. The largest separation between T_g and T_x (~200°C) occurs for a glass with initial 50% mullite concentration.

(5) These observations allow us to tune the initial glass composition to generate desired sequences and combinations of La-monazite and mullite crystalline combinations and morphologies, at the micro- to nanoscale, by applying scheduled heat treatments to the fully dense REAPS glass precursors.

(6) We have obtained initial evidence from our DSC investigations that compositional unmixing may also accompany or precede the crystallization events from the supercooled liquid state. Those could give rise to additional control parameters for CMC textures and formation.

Acknowledgements

This research was supported by AFOSR under Grant No. F49550-04-0153. We acknowledge the use of facilities within the LeRoy Eyring Center for Solid State Science at Arizona State University. Contributions of PFM to this project were supported by the UK Engineering and Physical Sciences Research Council.

References[40]

[1] J.B. Davis, R.S. Hay, D.B. Marshall, P.E.D. Morgan, A. Sayir, Influence of interfacial roughness on fiber sliding in oxide composites with La-monazite interphases, J. Amer. Ceram. Soc., 86 (2003) 305-316.

[2] J.B. Davis, D.B. Marshall, P.E.D. Morgan, Monazite-containing oxide/oxide composites, J. Eur. Ceram. Soc., 20 (2000) 583-587.

[3] P.E.D. Morgan, D.B. Marshall, Ceramic composites of monazite and alumina, J. Amer. Ceram. Soc., 78 (1995) 1553-1563.

[4] A.R. Barron, Mullite and Mullite Ceramics by H. Schneider, K. Okada and J. Pask, 1995.

[5] J.C. Lorrison, K.W. Dalgarno, D.J. Wood, Processing of an apatite-mullite glass-ceramic and an hydroxyapatite/phosphate glass composite by selective laser sintering, Journal of Materials Science: Materials in Medcine, 16 (2005) 775-781.

[6] H. Fathi, A. Johnson, R. van Noort, J.M. Ward, The influence of calcium fluoride (CaF2) on biaxial flexural strength of apatite-mullite glass-ceramic materials, Dental Materials, 21 (2005) 846-851.

[7] P. Mechnich, M. Schmuecker, H. Schneider, Stability of mullite-precursor versus potential fiber-coating material, High Temperature Ceramic Matrix Composites, [International Conference on High Temperature Ceramic Matrix Composites], 4th, Munich, Germany, Oct. 1-3, 2001, (2001) 164-167.

[8] J.B. Davis, D.B. Marshall, R.M. Housley, P.E.D. Morgan, Machinable ceramics containing rare-earth phosphates, J. Amer. Ceram. Soc., 81 (1998) 2169-2175.

[9] S. Guo, Glass formation and crystallization in the alumina-silica-lanthanum phosphate system for ceramics composites, in: Journal of the American Ceramic Society, Arizona State University, Tempe, 2006, pp. 174.

[10] R. Dupree, D. Holland, M.G. Mortuza, J.A. Collins, M.W.G. Lockyer, Magic-angle-spinning NMR of alkali phosphoaluminosilicate glasses, J. Non-Cryst. Solids, 112 (1989) 111-119.

[11] D.R. Tallant, C. Nelson, Raman investigation of glass structures in the sodium oxide-silica-phosphorus pentoxide-aluminum oxide system, Phys. Chem. Glasses, 27 (1986) 75-79.

[12] G.D. Cody, B. Mysen, G. Saghi-Szabo, J.A. Tossell, Silicate-phosphate interactions in silicate glasses and melts: I. A multinuclear (27Al,29Si,31P) MAS NMR and ab initio chemical shielding (31P) study of phosphorous speciation in silicate glasses, Geochim Cosmochim. Acta, 65 (2001) 2395-2411.

[13] M. Sitarz, M. Handke, Z. Fojud, S. Jurga, Spectroscopic studies of glassy phospho-silicate materials, J. Mol. Struct., 744-747 (2005) 621-626.

[14] H. Gan, P.C. Hess, Phosphate speciation in potassium aluminosilicate glasses, Am. Mineral., 77 (1992) 495-506.

[15] M.J. Toplis, T. Schaller, A ^{31}P MAS NMR study of glasses in the system xNa_2O-$(1-x)Al_2O_3$-$2SiO_2$-yP_2O_5, J. Non-Cryst. Solids, 224 (1998) 57-68.

[16] M.J. Toplis, B. Reynard, Temperature and time-dependent changes of structure in phosphorus containing aluminosilicate liquids and glasses: in situ Raman spectroscopy at high temperature, J. Non-Cryst. Solids, 263&264 (2000) 123-131.

[17] T. Schaller, J.F. Stebbins, The Structural Role of Lanthanum and Yttrium in Aluminosilicate Glasses: A 27Al and 17O MAS NMR Study, J. Phys. Chem. B, 102 (1998) 10690-10697.

[18] S. Boucher, J. Piwowarczyk, R.F. Marzke, B. Takulapalli, G.H. Wolf, P.F. McMillan, W.T. Petuskey, Melt and glass structure in the Al2O3-CaO-LaPO4 system studied by 27Al and 31P NMR, and by Raman scattering, J. Eur. Ceram. Soc., 25 (2005) 1333-1340.

[19] M.C. Wilding, P.F. McMillan, Polyamorphic transitions in yttria-alumina liquids, J. Non-Cryst. Solids, 293-295 (2001) 357-365.

[20] M.C. Wilding, P.F. McMillan, A. Navrotsky, Calorimetric Study of Glasses and liquids in the Polyamorphic system Y2O3-Al2O3, Phys. Chem. Glasses, 43 (2002) 306-312.

[21] P.F.M. Shuling Guo, William T. Petuskey, Preparation and characterization of alumina-rich Al2O3-AlPO4 glasses, J. Amer. Ceram. Soc., (2009).

[22] P. McMillan, B. Piriou, The structures and vibrational spectra of crystals and glasses in the silica-alumina system, J. Non-Cryst. Solids, 53 (1982) 279-298.

[23] M. Okuno, N. Zotov, M. Schmuecker, H. Schneider, Structure of SiO2-Al2O3 glasses: Combined X-ray diffraction, IR and Raman studies, J. Non-Cryst. Solids, 351 (2005) 1032-1038.

[24] B.T. Poe, P.F. McMillan, C.A. Angell, R.K. Sato, Aluminum and silicon coordination in silica-alumina glasses and liquids: a study by NMR and IR spectroscopy and MD simulations, Chem. Geol., 96 (1992) 333-349.

[25] S.H. Risbud, R.J. Kirkpatrick, A.P. Taglialavore, B. Montez, Solid-State NMR Evidence of 4-, 5- and 6-fold Aluminum Sites in Roller-Quenched SiO2-Al2O3 Glasses, J. Amer. Ceram. Soc., 70 (2005) C10-C12.

[26] N. Suriyanaraynan, K.V. Kannan Nithin, E. Bernado, Mullite Glass Ceramics Production from Coal Ash and Alumina by High Temperature Plasma, Journal of Non-Oxide Glasses, 1 (2009) 247-260.

[27] M. Schmuecker, K.J.D. MacKenzie, H. Schneider, R. Meinhold, NMR studies on rapidly solidified SiO2-Al2O3 and SiO2-Al2O3-Na2O-glasses, J. Non-Cryst. Solids, 217 (1997) 99-105.

[28] M. Schmuecker, H. Schneider, M. Poorteman, F. Cambier, R. Meinhold, Constitution of mullite glasses produced by ultra-rapid quenching of plasma-sprayed melts, J. Eur. Ceram. Soc., 15 (1995) 1201-1205.

[29] E. Lippmaa, M. Maegi, A. Samoson, G. Engelhardt, A.R. Grimmer, Structural studies of silicates by solid-state high-resolution silicon-29 NMR, Journal of the American Chemical Society, 102 (1980) 4889-4893.

[30] T.L. Weeding, B.H.W.S. De Jong, W.S. Veeman, B.G. Aitken, Silicon coordination changes from 4-fold to 6-fold on devitrification of silicon phosphate glass, Nature, 318 (1985) 352-353.

[31] R. Dupree, D. Holland, M.G. Mortuza, Six-coordinated silicon in glasses, Nature, 328 (1987) 416-417.

[32] C.S. Blackwell, R.L. Patton, Aluminum-27 and phosphorus-31 nuclear magnetic resonance studies of aluminophosphate molecular sieves, J. Phys. Chem., 88 (1984) 6135-6139.

[33] B. Glorieux, M. Matecki, F. Fayon, J.P. Coutures, S. Palau, A. Douy, G. Peraudeau, Study of lanthanum orthophosphates polymorphism, in view of actinide conditioning, J. Nucl. Mater., 326 (2004) 156-162.

[34] Y. Zhang, A. Navrotsky, Thermochemistry of rare-earth aluminate and aluminosilicate glasses, J. Non-Cryst. Solids, 341 (2004) 141-151.

[35] Y. Zhang, A. Navrotsky, Thermochemistry of glasses in the Y2O3-Al2O3-SiO2 system, J. Amer. Ceram. Soc., 86 (2003) 1727-1732.

[36] Y. Zhang, A. Navrotsky, J.A. Tangeman, J.K.R. Weber, Thermochemistry of glasses along the 2NdAlO3-3SiO2 join, J. Phys. Cond. Mat., 15 (2003) S2343-S2355.

[37] A. Navrotsky, K.L. Geisinger, P. McMillan, G.V. Gibbs, The tetrahedral framework in glasses and melts - inferences from molecular orbital calculations and implications for structure, thermodynamics, and physical properties, Phys. Chem. Minerals, 11 (1985) 284-298.

[38] McMillan, Glass-ceramics, 2nd ed., Academic Press, 1979.

[39] N.J. Clayden, S. Esposito, A. Aronne, P. Pernice, Solid state 27Al NMR and FTIR study of lanthanum aluminosilicate glasses, J. Non-Cryst. Solids, 258 (1999) 11-19.

[40] P. Mechnich, M. Schmuecker, H. Schneider, Stability of mullite-precursor versus potential fiber-coating material, in: High Temperature Ceramic Matrix Composites, [International Conference on High Temperature Ceramic Matrix Composites], 4th, Munich, Germany, 2001, pp. 164-167.

Table 1. Glass composition, density (ρ), glass transition (T_g) and crystallization temperatures (T_x; T_{x1}, T_{x2}) of $3Al_2O_3 \cdot 2SiO_2$-$LaPO_4$ glasses. The composition of the starting mixture is given in mol% mullite and $LaPO_4$ as well as oxide components, whereas the final analyzed glass compositions are shown as mol% oxides.

Fig. 1. X-ray powder diffraction patterns of $3Al_2O_3 \cdot 2SiO_2$-$LaPO_4$ glasses obtained by quenching from the melt using the containerless technique. Note that sample designations correspond to the starting compositions. The analyzed values are generally slightly (<15%) lower in P_2O_5 content, although the Al:Si ratio remains the same. The sharp diffraction peaks observed for the partly crystallized 20% mullite sample correspond to $LaPO_4$ monazite.

Fig. 2. $3Al_2O_3 \cdot 2SiO_2$-$LaPO_4$ glass density as a function of composition, compared with the compositionally averaged density of crystalline La-monazite and mullite mixtures.

Fig. 3. DSC traces of $3Al_2O_3 \cdot 2SiO_2$-$LaPO_4$ glasses obtained using scan rate 20° C/min. (a) Glasses with <50 mol% mullite component; (b) Glasses with >50 mol% mullite component. Series (a) and (b) are distinguished by the appearance of two (T_{x1}, T_{x2}) *vs* one (T_x) crystallization exotherm.

Fig. 4. Glass transition and crystallization temperature of $3Al_2O_3 \cdot 2SiO_2$-$LaPO_4$ glasses reported as a function of glass composition in terms of the initial mullite component concentrations.

Fig. 5. Solid state MAS NMR spectra of $3Al_2O_3 \cdot 2SiO_2$-$LaPO_4$ glasses. (a) ^{27}Al MAS NMR spectra; (b) ^{29}Si MAS NMR spectra ; (c) ^{31}P MAS NMR spectra of $3Al_2O_3 \cdot 2SiO_2$-$LaPO_4$ glasses.

Fig. 6. ^{31}P NMR chemical shift as a function of $LaPO_4$ content for $3Al_2O_3 \cdot 2SiO_2$-$LaPO_4$ glasses.

Fig. 8. Raman spectra of $3Al_2O_3 \cdot 2SiO_2$-$LaPO_4$ glasses.

Fig. 9. Structural model for a typical $3Al_2O_3 \cdot 2SiO_2$-$LaPO_4$ glass developed at the $50(3Al_2O_3 \cdot 2SiO_2) \cdot 50LaPO_4$ composition from NMR and Raman data.

Table 1. Glass composition, density, glass transition (Tg) and crystallization temperatures (Tx) of $3Al_2O_3 \cdot 2SiO_2$-$LaPO_4$ glasses.

Starting (mol%)		Nominal (mol%)				Analyzed (mol%)				Tg	Tx_1	Tx_2	ρ
mullite	$LaPO_4$	Al_2O_3	SiO_2	P_2O_5	La_2O_3	Al_2O_3	SiO_2	P_2O_5	La_2O_3		(°C)		g/cm^3
20.0	80.0	33.3	22.2	22.2	22.2						903	987	
25.0	75.0	37.5	25.0	18.8	18.8	39.7	27.0	15.9	17.4	845	917	987	3.76
30.0	70.0	40.9	27.3	15.9	15.9	42.6	28.5	13.2	15.7	860	930	993	3.62
35.0	65.0	43.8	29.2	13.5	13.5	43.7	29.5	13.0	13.8	863	959	998	3.49
40.0	60.0	46.2	30.8	11.5	11.5	47.0	31.5	10.5	10.9	862		1047	3.36
50.0	50.0	50.0	33.3	8.3	8.3	49.5	33.1	9.3	8.1	879		1065	3.22
60.0	40.0	52.9	35.3	5.9	5.9	53.7	35.7	5.3	5.4	886		1058	3.09
75.0	25.0	56.3	37.5	3.1	3.1	57.4	37.7	2.3	2.6	908		1019	2.96
80.0	20.0	57.1	38.1	2.4	2.4	57.5	38.1	2.0	2.4	906		1015	2.94
100.0	0.0	60.0	40.0	0.0	0.0	60.1	39.9	0.0	0.0			992	2.82

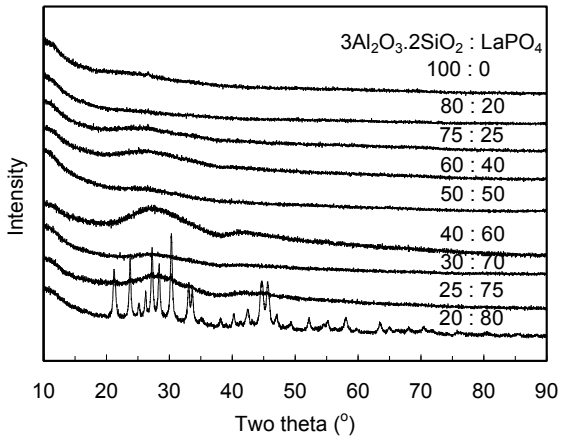

Fig. 1. X-ray powder diffraction patterns of $3Al_2O_3 \cdot 2SiO_2$-$LaPO_4$ glasses obtained by quenching from the melt using the containerless technique.

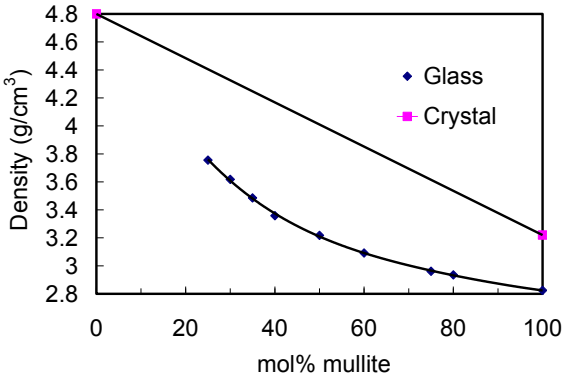

Fig. 2. $3Al_2O_3 \cdot 2SiO_2$-$LaPO_4$ glass density as a function of composition, compared with the compositionally averaged density of crystalline La-monazite and mullite mixtures.

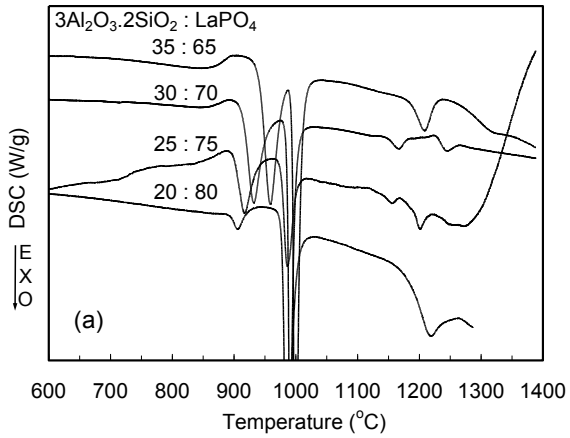

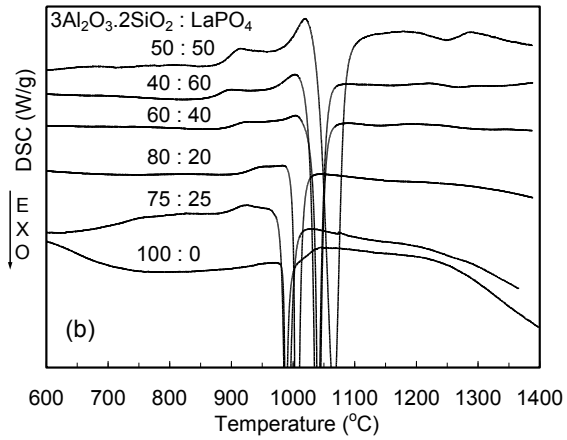

Fig. 3. DSC traces of $3Al_2O_3 \cdot 2SiO_2$-$LaPO_4$ glasses obtained using scan rate 20° C/min. (a) Glasses with <50 mol% mullite component; (b) Glasses with >50 mol% mullite component.

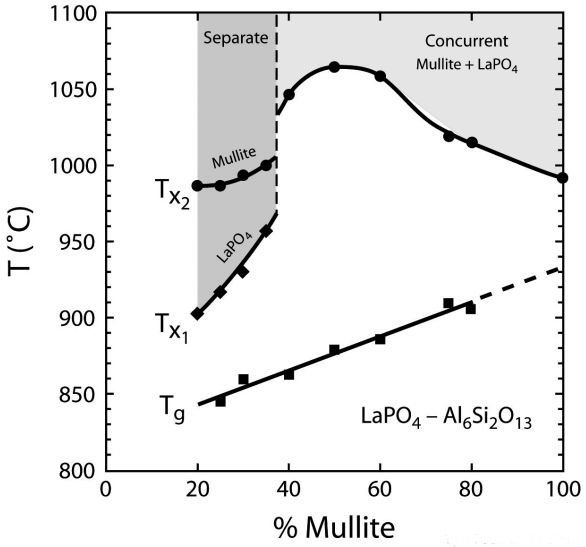

Fig. 4. Glass transition and crystallization temperature of $3Al_2O_3 \cdot 2SiO_2$-$LaPO_4$ glasses as a function of glass composition.

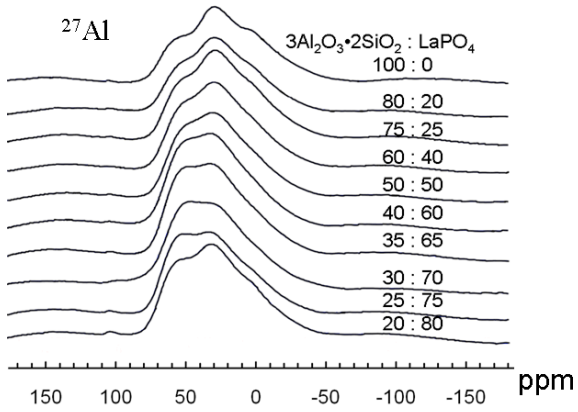

(a)

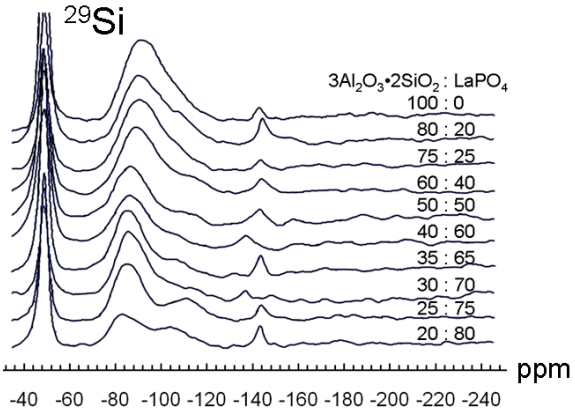

(b)

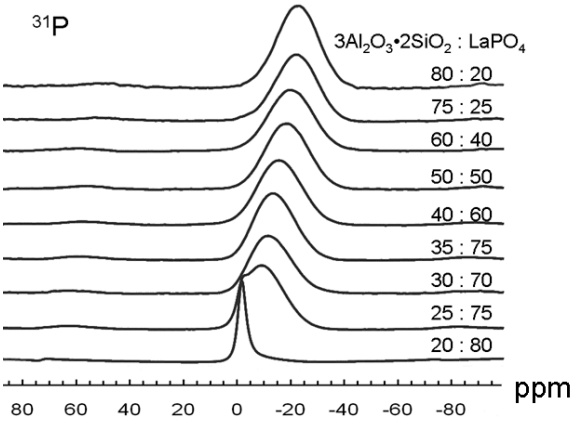

(c)

Fig. 5. Solid state MAS NMR spectra of $3Al_2O_3 \cdot 2SiO_2$-$LaPO_4$ glasses. (a) ^{27}Al MAS NMR spectra; (b) ^{29}Si MAS NMR spectra ; (c) ^{31}P MAS NMR spectra of $3Al_2O_3 \cdot 2SiO_2$-$LaPO_4$ glasses.

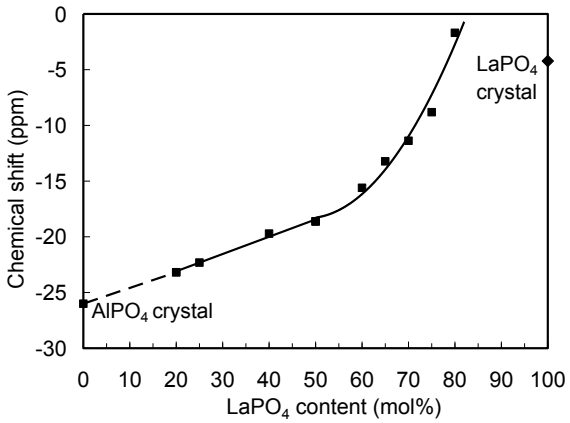

Fig. 6. ^{31}P NMR chemical shift as a function of $LaPO_4$ content for $3Al_2O_3 \cdot 2SiO_2$-$LaPO_4$ glasses.

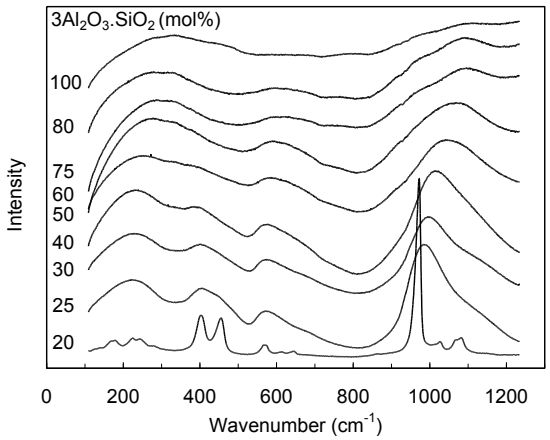

Fig. 7. Raman spectra of $3Al_2O_3 \cdot 2SiO_2$-$LaPO_4$ glasses.

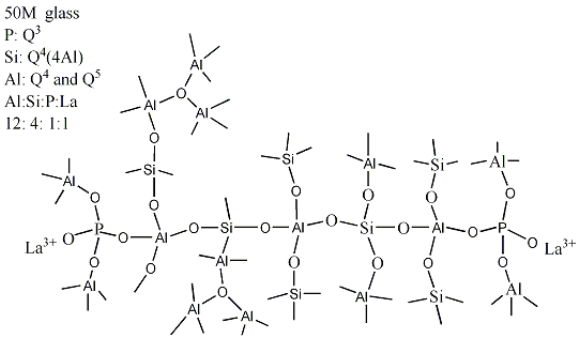

Fig. 8. A structural model for a typical $3Al_2O_3 \cdot 2SiO_2$-$LaPO_4$ glass developed at the $50(3Al_2O_3 \cdot 2SiO_2) \cdot 50LaPO_4$ composition, based on input from NMR and Raman data.